Letter

Quasiparticle characteristics of the weakly ferromagnetic Hund metal MnSi

Yuan Fang,[1,*] Huali Zhang,[1,*] Ding Wang,[1,*] Guowei Yang,[1] Yi Wu,[1] Peng Li,[1] Zhiguang Xiao,[1] Tianyun Lin,[1] Hao Zheng,[1] Xiao-Long Li,[2] Huan-Hua Wang,[3] Fanny Rodolakis,[4] Yu Song,[1] Yilin Wang,[5] Chao Cao,[1] and Yang Liu[1,6,7,†]

[1]*Center for Correlated Matter and Department of Physics, Zhejiang University, Hangzhou 310058, China*
[2]*Shanghai Synchrotron Radiation Facility, Shanghai Advanced Research Institute, Chinese Academy of Sciences, Shanghai 201204, China*
[3]*Institute of High Energy Physics, Chinese Academy of Sciences, Beijing 100049, China*
[4]*Advanced Photon Source, Argonne National Laboratory, 9700 South Cass Avenue, Argonne, Illinois 60439, USA*
[5]*Hefei National Laboratory for Physical Sciences at Microscale, University of Science and Technology of China, Hefei, Anhui 230026, China*
[6]*Zhejiang Province Key Laboratory of Quantum Technology and Device, Zhejiang University, Hangzhou, China*
[7]*Collaborative Innovation Center of Advanced Microstructures, Nanjing University, Nanjing 210093, China*

(Received 20 June 2022; revised 26 September 2022; accepted 12 October 2022; published 25 October 2022)

Hund metals are multiorbital systems with 3*d* or 4*d* electrons exhibiting both an itinerant character and local moments, and they feature Kondo-like screenings of local orbital and spin moments, with suppressed coherence temperatures driven by Hund's coupling J_H. They often exhibit magnetic order at low temperature, but how the interaction between the Kondo-like screening and long-range magnetic order is manifested in the quasiparticle spectrum remains an open question. Here, we present the spectroscopic signature of such an interaction in a Hund metal candidate MnSi exhibiting weak ferromagnetism. Our photoemission measurements reveal renormalized quasiparticle bands near the Fermi level with strong momentum dependence: The ferromagnetism manifests through possibly exchange-split bands (Q1) below T_C, while the spin/orbital screenings lead to the gradual development of quasiparticles (Q2) upon cooling. Our results demonstrate how the characteristic spin/orbital coherence in a Hund metal could coexist and compete with the magnetic order to form a weak itinerant ferromagnet, via quasiparticle bands that are well separated in momentum space and exhibit distinct temperature dependence. Our results imply that the competition between the spin/orbital screening and the magnetic order in a Hund metal bears interesting similarities to the Kondo lattice systems.

DOI: 10.1103/PhysRevB.106.L161112

Understanding weak itinerant ferromagnets represents an outstanding question in condensed matter physics [1,2]. In these materials, the ordered moments in the ferromagnetic (FM) phase are much smaller than the local moments inferred from the Curie-Weiss law above the Curie temperature T_C, which indicates that models based on the local-moment physics (e.g., the Heisenberg model) do not hold. On the other hand, a simple itinerant band picture is also inadequate, as it does not capture the effects due to spin fluctuations and electronic correlations. As an archetypal weak ferromagnet, MnSi plays an important role in the understanding of weak ferromagnetism and validating the famous spin fluctuation theory by Moriya [3]. Nevertheless, the importance of electron correlation and the underlying mechanism of coexisting local moments and itinerant electrons remain open questions.

In multiorbital (3*d* or 4*d*) weak ferromagnets, strong electron correlations could arise from the interorbital Hund's coupling J_H, leading to the so-called Hund metal (HM) [4–8]. The HM physics is thought to play an important role in many correlated electron systems, including iron pnictides, ruthenates, transition metal chalcogenides, etc. [4–15]. A recent study from inelastic neutron scattering (INS) and dynamic mean-field theory (DMFT) suggested that MnSi is a HM exhibiting strong orbital and spin fluctuations [16], which can be crucial for its non-Fermi-liquid behaviors over a large phase space [17–20]. It was further proposed that the orbital coherence scale might be smaller than the spin one in MnSi, implying possibly an unconventional type of HM as a result of strong electron correlations [16]. A key characteristic of the HM is the quasiparticle (QP) bands that emerge gradually at low temperature, due to the low coherence temperature, but these QP bands remain elusive in MnSi. In addition, how the QP coherence as a result of the HM physics interacts with the weak FM is another interesting question. While a previous study from angle-resolved photoemission spectroscopy (ARPES) on bulk MnSi(001) suggested weak electron correlation [21], another ARPES study on thick MnSi(111) films emphasized the importance of Fermi-surface (FS) nesting in driving the strong magnetic fluctuations [22]. Nevertheless, neither the FM exchange splitting below T_C nor the characteristic QP bands as a result of the HM physics have been identified so far.

*These authors contributed equally to this work.
†yangliuphys@zju.edu.cn

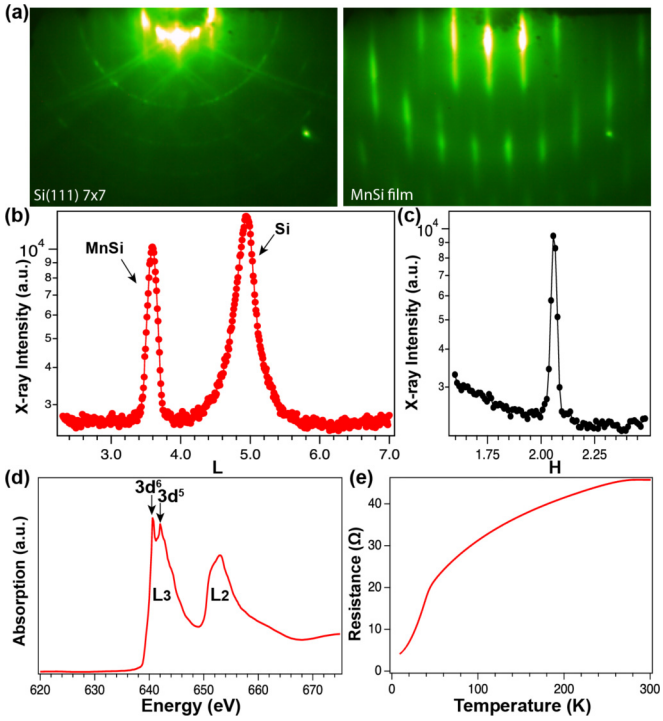

FIG. 1. Characterization of MnSi films. (a) RHEED patterns of the Si(111)-7 × 7 surface and a typical MnSi film. (b), (c) X-ray diffraction scans of a thick MnSi film near the MnSi Bragg peak centered at $(H, K, L) = (2.069, 0, 3.582)$, where H, K, L are defined in units of Si substrate [23]. (d) XAS spectrum near the Mn L edge taken at 29 K. (e) Resistance vs temperature for a MnSi film, showing a kink at $T_C \sim 45$ K.

Here, combining thin film growth by molecular beam epitaxy (MBE) and *in situ* electronic structure measurements by ARPES, we demonstrate the QP characteristics of the weakly ferromagnetic HM MnSi. Our MnSi films were grown on Si(111) substrates and transferred under ultrahigh vacuum to a helium-lamp ARPES system for electronic structure measurements. Details can be found in the Supplemental Material (SM) [23] (see also Refs. [24–26] therein). Figure 1(a) shows the reflection high-energy electron diffraction (RHEED) patterns from the starting Si(111)-7 × 7 surface and an as-grown thick MnSi film, confirming epitaxial growth of high-quality MnSi films. The epitaxial growth is further confirmed by *ex situ* x-ray scattering measurements [Figs. 1(b) and 1(c)], showing that the in-plane and out-of-plane lattice constants are ∼3.243 and ∼7.872 Å, respectively [23]. This indicates that the epitaxial MnSi film undergoes a tensile strain of ∼1% compared to bulk MnSi, although it does not fully match with the underlying Si substrate, similar to previous studies [22,27]. The strain gives rise to an enhanced $T_C \sim 45$ K (compared to $T_C \sim 30$ K in bulk MnSi), as evidenced by the characteristic kink in the resistance versus temperature data shown in Fig. 1(e). Due to the noncentrosymmetric crystal structure, there is a weak Dzyaloshinskii-Moriya (DM) interaction which leads to a very small rotation (∼5°) of the in-plane Mn moments between the adjacent (111) planes [28]. However, the DM interaction is too weak to generate any obvious effect on the observed QP bands (see Fig. S1 in SM [23]), and therefore is ignored in this Letter. Measurements from x-ray absorption spectroscopy (XAS) near the Mn L edge indicate that the ground state is mixed valent with both $3d^5$ and $3d^6$ configurations, similar to bulk MnSi [29]. The presence of the $3d^6$ configuration is unusual for Mn and is likely caused by hybridization with Si orbitals. Note that the $3d^6$ configuration is one electron more than half filling, implying an important role of Hund's physics [16].

Figure 2(a) shows the energy-momentum dispersion taken with He I (21.2 eV) and He II (40.8 eV) photons, revealing dispersive QP bands near the Fermi level (E_F). For comparison, Fig. 2(b) shows the calculated band structure from density functional theory (DFT) overlaid on top of the ARPES data, with $k_z = 0.4$ and 1.196 Å^{-1} based on an estimated inner potential of ∼12.8 eV (see Fig. S2 in SM [23] for more details). The Mn moment was set to the experimental value of $0.4\mu_B$/Mn in DFT calculations [30], which yields a FM exchange splitting of ∼0.2 eV (see Fig. S3 in SM [23]). The overall valence bands from the 21.2 eV data can be partially explained by the DFT calculations, particularly the broad parabolic band near −1.2 eV (labeled B1) centered at $\bar{\Gamma}$ and the holelike bands near E_F (labeled B2) centered at $k_y \sim 1.12$ Å^{-1}, i.e., $\bar{\Gamma}$ in the second surface Brillouin zone (BZ). For the 40.8 eV data, different set of bands [labeled B3, B4 in Fig. 2(a)] can be observed. The obvious spectral difference between the first and second surface BZs confirms that the observed spectral features are bulk states, as the bulk BZ is twice as large as the surface BZ [see Fig. 2(b)]. Despite these similarities between ARPES results and DFT calculations, the ARPES spectra also show well-defined flat bands right near E_F extending over a large momentum region (±0.6 Å^{-1}), marked by black arrows in Figs. 2(c) and 2(d), which cannot be easily accounted for by DFT calculations. We mention that DMFT calculations indeed suggest enhanced effective mass (or flatness) of quasiparticle bands near E_F compared to DFT [16], although they cannot reproduce quantitatively the pronounced flat bands observed experimentally (note that DMFT calculations in Ref. [16] were performed at room temperature). In addition, the experimental constant energy maps [Fig. 2(e)] show obvious deviations from the DFT calculations (see Fig. S4 in SM [23]). Such a discrepancy implies appreciable band renormalization near E_F, suggesting that correlation effects are likely important in MnSi. The flat QP bands near E_F are consistent with the enhanced effective mass from de Haas–van Alphen [31,32] and specific heat measurements [33,34]. Note that the QP bands are well defined near E_F and become much broader away from E_F, in agreement with the strong QP scattering as a result of the correlation effect.

To understand the electron correlation from the HM physics and the origin of FM, the temperature evolution of the QP bands is crucial. Figure 3(a) shows the momentum-dependent energy distribution curves (EDCs) along the $\bar{\Gamma}$-$\bar{M}$ direction above and below T_C, where clear spectral changes across T_C with strong momentum dependence can be observed. In particular, near $k_y \sim 1.118$ Å^{-1} [Fig. 3(b)], there is a broad asymmetric peak (Q1) at ∼−0.15 eV in the paramagnetic (PM) phase (see the 80 K data), which evolves into two peaks at ∼−0.3 and ∼−0.15 eV in the FM phase, and at the same time, the spectral weight at E_F is reduced (see the 6 K

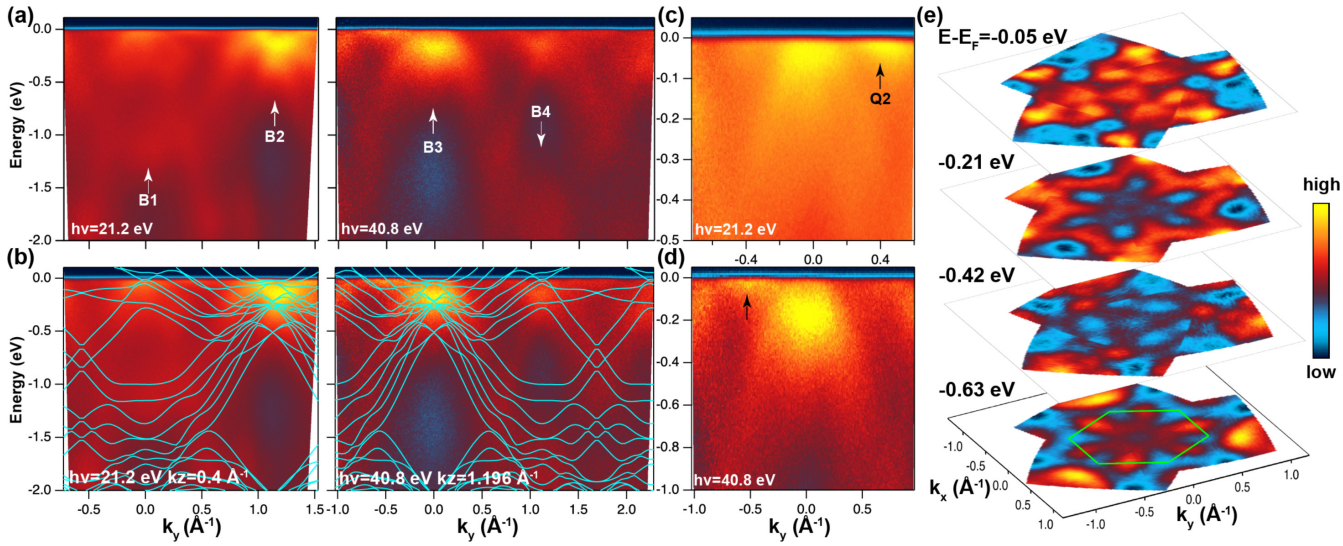

FIG. 2. ARPES spectra of MnSi films taken at ∼6 K. (a) ARPES data of a MnSi film taken with 21.2 and 40.8 eV photons, measured along $\bar{\Gamma}$-$\bar{M}$. (b) Results from DFT calculations overlaid on top of ARPES data. The k_z values are based on an estimated inner potential of ∼12.8 eV. (c), (d) Zoomed-in view of the QP bands near E_F. Black arrows highlight flat QP bands near E_F. (e) Constant energy maps at various energies using 21.2 eV photons. The green hexagon at the bottom marks the surface BZ.

data). According to DFT calculations in the PM phase (see Fig. S3(a) in SM [23]), the broad asymmetric Q1 peak could contain contributions from two close-by bands, i.e., Q1-1 at ∼−0.15 eV and Q1-2 very close to E_F. Upon entering the FM phase, the FM exchange splittings of Q1-1 and Q1-2 could lead to emergence of a new satellite band at ∼−0.3 eV (from the majority band of Q1-1), a more pronounced central peak at ∼−0.15 eV (due to overlapping contributions from

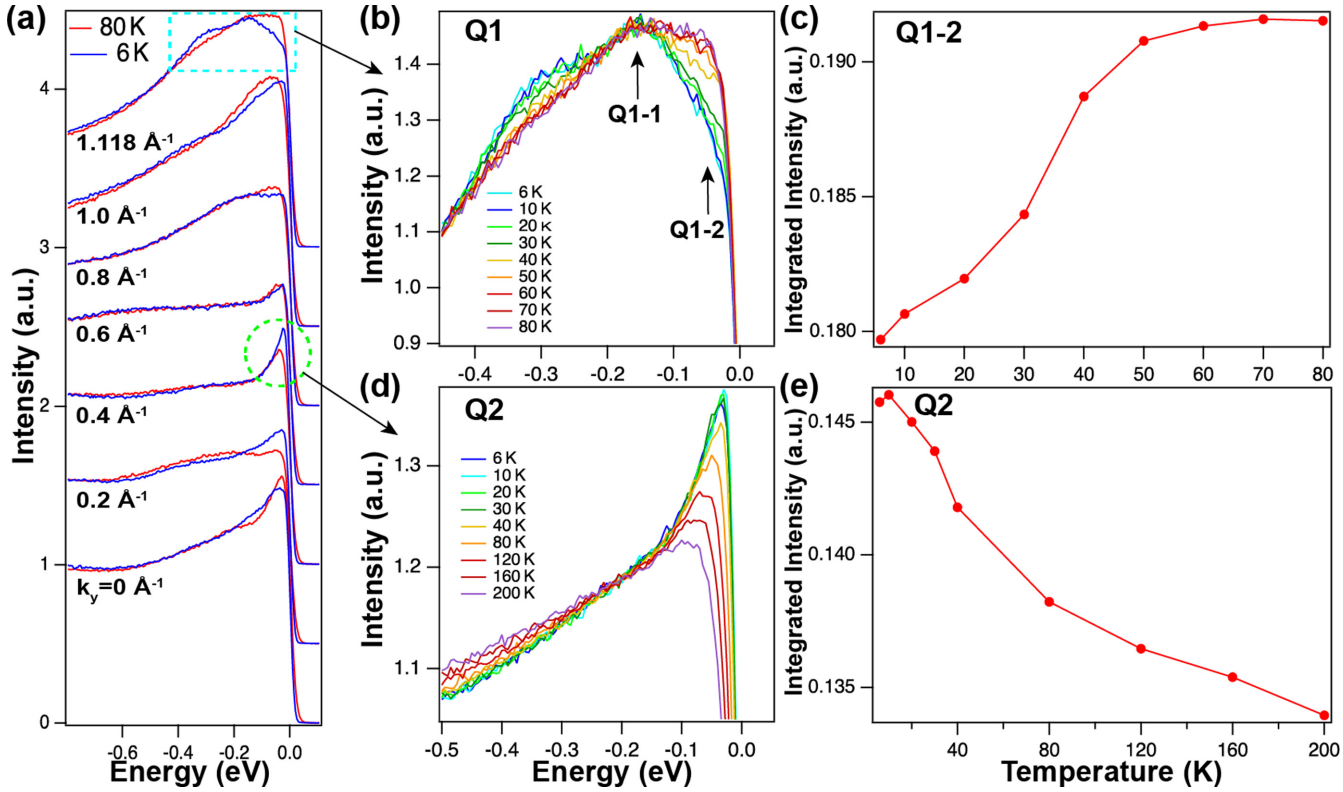

FIG. 3. Temperature evolution of QP bands. (a) Momentum-dependent EDCs well below (blue curves, ∼6 K) and above T_C (red curves, ∼80 K) along the $\bar{\Gamma}$-$\bar{M}$ direction. The cyan dashed box and green dashed circle highlight the Q1 [(b), (c)] and Q2 [(d), (e)] bands, respectively. (b), (d) Temperature evolution of the EDCs. (c), (e) The integrated intensity of (c) Q1-2 and (e) Q2 from (b) and (d) as a function of temperature. The integration region is [−0.145 eV, −0.01 eV] for Q1-2 and [−0.125 eV, 0.005 eV] for Q2.

split Q1-1 and Q1-2 peaks), and reduced density of states (DOS) at E_F (as the minority band of Q1-2 is pushed above E_F). See Fig. S6 in SM [23] for a schematic illustration of our proposed scenario. Detailed temperature-dependent scans [Figs. 3(b) and 3(c)] further show that this temperature-driven transition takes place near $T_C \sim 45$ K, consistent with its FM origin. Although our interpretation of the Q1 temperature evolution in terms of FM exchange splitting is the most plausible one based on current data, other possibilities cannot be completely ruled out. In contrast to a momentum-independent FM exchange splitting of ∼0.2 eV obtained from DFT calculations [23], the experimental FM splitting seems to be highly anisotropic in momentum space. For instance, the QP band near $k_y \sim 0.6$ Å^{-1} shows almost no sign of FM splitting, while the EDCs at $k_y \sim 0.4$ and 0.2 Å^{-1} show the opposite trend compared to that at $k_y \sim 1.118$ Å^{-1} [Fig. 3(a)], i.e., the spectral weight is now transferred from deeper energies to E_F upon cooling. This leads to the development of a sharp quasiparticle peak near E_F at low temperature, e.g., the Q2 peak at $k_y \sim 0.4$ Å^{-1}.

Although it is tempting to attribute the observed momentum anisotropy to momentum-dependent FM exchange splitting, as observed in some FM systems [35–37], the gradual enhancement of the Q2 peak upon cooling over a wide temperature range implies that its spectral change is not caused by the FM order [Fig. 3(d)]. Instead, such behavior is consistent with the QPs expected in a HM, i.e., QPs with low coherence temperature and energy scale. The suppressed coherence temperature is due to Hund's coupling, i.e., large Hund's coupling will help the formation of large local moments with a low coherence temperature [8]. Interestingly, the growth of the Q2 peak appears to slow down below ∼30 K, as shown in Fig. 3(d). To recover the full spectral function near E_F, we divide the temperature-dependent EDCs by the resolution-convoluted Fermi-Dirac function (for details, see Fig. S5 in SM [23]). The integrated peak intensity after such an analysis is summarized in Fig. 3(e), which indicates that the peak intensity grows monotonically above T_C, and shows sign of slowing down well below T_C [23].

It is interesting to note that the Q2 QP development at low temperature is limited to a small energy region near E_F [Fig. 3(d)], and its intensity over a wide temperature range can be roughly described by the $-\log(T)$ dependence (Fig. S5 in SM [23]). These characteristics bear an intriguing similarity to the renowned Kondo resonances in Kondo lattice (KL) systems [38–41]. There, the spin-flip scattering of conduction electrons with the local moments leads to spin screening and a gradual buildup of the Kondo resonance near E_F. In the HM, the screening could occur in both the spin and orbital channels [16,42], with separated energy scales, which can give rise to QP bands with a strong temperature dependence, as exemplified in ruthenates [12–14,43]. The low coherence energy also results in a broad regime with bad metal or non-Fermi-liquid (NFL) behaviors [44]. Indeed, MnSi is well known for its extended NFL region over a large pressure/temperature region [17–20].

The possible slowdown of the Q2 QP development below T_C [see Fig. S5(i) in SM [23]] suggests that the QP coherence as a result of orbital/spin screening might be interrupted by the FM order. This implies an interesting analogy to the f-electron KL systems: There, the magnetic order (via the Ruderman-Kittel-Kasuya-Yosida (RKKY) exchange interaction) competes with the heavy QP formation (via the Kondo screening), resulting in the well-known Doniach phase diagram that lies at the heart of the heavy fermion physics [45]. Often, magnetic KL systems exhibit some degree of Kondo screening, and recent ARPES studies on CeSb and USb_2 indicate that the competition between the RKKY and Kondo interactions is manifested by the momentum-separated QP bands [46,47]. The itineracy of the f electrons can be estimated by the magnitude of the screened moment, i.e., the ratio between the local moment above T_C and the ordered moment below T_C. In bulk MnSi, this ratio is ∼5 [28,48]: Such a moderately large value is probably a direct consequence of the competition between the spin/orbital screening from the HM physics and the long-range FM order. Our results therefore suggest that the FM order and the spin/orbital screening can coexist and compete in a multiorbital $3d$ HM, via momentum-separated QP bands with a distinct temperature dependence, resulting in a weak itinerant ferromagnet. Such insight might help explain the dichotomy of itinerant and local moments observed in recent INS studies [16,49].

To conclude, we present systematic temperature-dependent ARPES results for a HM candidate MnSi with weak FM. We observed well-defined QP bands with a pronounced temperature dependence: The Q1 band shows a possible FM exchange splitting below T_C, originating from its weak itinerant FM; by contrast, the Q2 peak grows monotonically upon cooling above T_C, and becomes fully developed inside the FM phase, as a result of the characteristic orbital/spin screening in a HM. Our results therefore provide spectroscopic insight for understanding the coexistence and competition between the weak FM (forming ordered moments) and the HM physics (favoring screened moments at low temperature): It can be achieved through QP bands that are well separated in momentum space and exhibit distinct temperature dependence. Such competition in a ferromagnetic HM bears striking similarity with the classical KL systems. Our study motivates future works to understand the underlying mechanism of the momentum-dependent electron correlation, as well as the inherent connection between the Kondo physics and HM physics. Interestingly, a very recent DMFT study shows that the QP self-energy can indeed exhibit strong momentum anisotropy in a multiorbital Hund ferromagnet [50].

This work is supported by the Key R&D Program of Zhejiang Province, China (2021C01002), the State Key project of Zhejiang Province (No. LZ22A040007), the National Science Foundation of China (No. 12174331, No. 11674280), the National Key R&D Program of China (Grants No. 2017YFA0303100 and No. 2016YFA0300203), and the Fundamental Research Funds for the Central Universities (2021FZZX001-03). The surface x-ray diffraction experiments were performed at Beamline 1W1A in Beijing Synchrotron Radiation Facility (BSRF) and Beamline BL02U2 in Shanghai Synchrotron Radiation Facility (SSRF). The XAS measurements were performed at 29-ID IEX beam-

line at Advanced Photon Source (APS). APS is supported by the U.S. Department of Energy (DOE) Office of Science under Contract No. DE-AC02-06CH11357; additional support by the National Science Foundation under Grant No. DMR-0703406 is also acknowledged. We thank Dr. Chenchao Xu, Professor Xin Lu, Professor Huiqiu Yuan, Professor Zhi-Cheng Zhong, and Professor Yi-feng Yang for experimental help and useful discussions.

[1] J. M. Santiago, C.-L. Huang, and E. Morosan, J. Phys.: Condens. Matter **29**, 373002 (2017).
[2] M. Brando, D. Belitz, F. M. Grosche, and T. R. Kirkpatrick, Rev. Mod. Phys. **88**, 025006 (2016).
[3] T. Moriya, *Spin Fluctuations in Itinerant Electron Magnetism* (Springer, Berlin, 1985).
[4] Z. P. Yin, K. Haule, and G. Kotliar, Nat. Mater. **10**, 932 (2011).
[5] Z. P. Yin, K. Haule, and G. Kotliar, Nat. Phys. **7**, 294 (2011).
[6] L. de'Medici, J. Mravlje, and A. Georges, Phys. Rev. Lett. **107**, 256401 (2011).
[7] J. Mravlje, M. Aichhorn, T. Miyake, K. Haule, G. Kotliar, and A. Georges, Phys. Rev. Lett. **106**, 096401 (2011).
[8] A. Georges, L. de' Medici, and J. Mravlje, Annu. Rev. Condens. Matter Phys. **4**, 137 (2013).
[9] M. Yi, D. H. Lu, R. Yu, S. C. Riggs, J.-H. Chu, B. Lv, Z. K. Liu, M. Lu, Y.-T. Cui, M. Hashimoto, S.-K. Mo, Z. Hussain, C. W. Chu, I. R. Fisher, Q. Si, and Z.-X. Shen, Phys. Rev. Lett. **110**, 067003 (2013).
[10] H. Miao, Z. P. Yin, S. F. Wu, J. M. Li, J. Ma, B.-Q. Lv, X. P. Wang, T. Qian, P. Richard, L.-Y. Xing, X.-C. Wang, C. Q. Jin, K. Haule, G. Kotliar, and H. Ding, Phys. Rev. B **94**, 201109(R) (2016).
[11] A. Damascelli, D. H. Lu, K. M. Shen, N. P. Armitage, F. Ronning, D. L. Feng, C. Kim, Z.-X. Shen, T. Kimura, Y. Tokura, Z. Q. Mao, and Y. Maeno, Phys. Rev. Lett. **85**, 5194 (2000).
[12] S.-C. Wang, H.-B. Yang, A. K. P. Sekharan, H. Ding, J. R. Engelbrecht, X. Dai, Z. Wang, A. Kaminski, T. Valla, T. Kidd, A. V. Fedorov, and P. D. Johnson, Phys. Rev. Lett. **92**, 137002 (2004).
[13] T. Kondo, M. Ochi, M. Nakayama, H. Taniguchi, S. Akebi, K. Kuroda, M. Arita, S. Sakai, H. Namatame, M. Taniguchi, Y. Maeno, R. Arita, and S. Shin, Phys. Rev. Lett. **117**, 247001 (2016).
[14] A. Tamai, M. Zingl, E. Rozbicki, E. Cappelli, S. Riccò, A. de la Torre, S. McKeown Walker, F. Y. Bruno, P. D. C. King, W. Meevasana, M. Shi, M. Radović, N. C. Plumb, A. S. Gibbs, A. P. Mackennzie, C. Berthod, H. U. R. Strand, M. Kim, A. Georges, and F. Baumberger, Phys. Rev. X **9**, 021048 (2019).
[15] B. G. Jang, G. Han, I. Park, D. Kim, Y. Y. Koh, Y. Kim, W. Kyung, H.-D. Kim, C.-M. Cheng, K.-D. Tsuei, K. D. Lee, N. Hur, J. H. Shim, C. Kim, and G. Kotliar, Nat. Commun. **12**, 1208 (2021).
[16] X. Chen, I. Krivenko, M. B. Stone, A. I. Kolesnikov, T. Wolf, D. Reznik, K. S. Bedell, F. Lechermann, and S. D. Wilson, Nat. Commun. **11**, 3076 (2020).
[17] C. Pfleiderer, S. R. Julian, and G. G. Lonzarich, Nature (London) **414**, 427 (2001).
[18] N. Doiron-Leyraud, I. R. Walker, L. Taillefer, M. J. Steiner, S. R. Julian, and G. G. Lonzarich, Nature (London) **425**, 595 (2003).
[19] C. Pfleiderer, D. Reznik, L. Pintschovius, H. v. Löhneysen, M. Garst, and A. Rosch, Nature (London) **427**, 227 (2004).
[20] R. Ritz, M. Halder, M. Wagner, C. Franz, A. Bauer, and C. Pfleiderer, Nature (London) **497**, 231 (2013).
[21] K. Kura, K. Takano, Y. Takeichi, A. Harasawa, T. Okuda, I. Matsuda, and A. Kakizaki, J. Phys. Soc. Jpn. **77**, 024709 (2008).
[22] A. Nicolaou, M. Gatti, E. Magnano, P. Le Fèvre, F. Bondino, F. Bertran, A. Tejeda, M. Sauvage-Simkin, A. Vlad, Y. Garreau, A. Coati, N. Guérin, F. Parmigiani, and A. Taleb-Ibrahimi, Phys. Rev. B **92**, 081110(R) (2015).
[23] See Supplemental Material at http://link.aps.org/supplemental/10.1103/PhysRevB.106.L161112 for details on thin film growth, ARPES measurements, and DFT calculations, which includes Refs. [24–26].
[24] B. Geisler, P. Kratzer, T. Suzuki, T. Lutz, G. Costantini, and K. Kern, Phys. Rev. B **86**, 115428 (2012).
[25] G. Kresse and J. Hafner, Phys. Rev. B **47**, 558 (1993).
[26] G. Kresse and D. Joubert, Phys. Rev. B **59**, 1758 (1999).
[27] E. Karhu, S. Kahwaji, T. L. Monchesky, C. Parsons, M. D. Robertson, and C. Maunders, Phys. Rev. B **82**, 184417 (2010).
[28] G. Shirane, R. Cowley, C. Majkrzak, J. B. Sokoloff, B. Pagonis, C. H. Perry, and Y. Ishikawa, Phys. Rev. B **28**, 6251 (1983).
[29] F. Carbone, M. Zangrando, A. Brinkman, A. Nicolaou, F. Bondino, E. Magnano, A. A. Nugroho, F. Parmigiani, T. Jarlborg, and D. van der Marel, Phys. Rev. B **73**, 085114 (2006).
[30] T. Jeong and W. E. Pickett, Phys. Rev. B **70**, 075114 (2004).
[31] L. Taillefer, G. G. Lonzarich, and P. Strange, J. Magn. Magn. Mater. **54-57**, 957 (1986).
[32] M. A. Wilde, M. Dodenhöft, A. Niedermayr, A. Bauer, M. M. Hirschmann, K. Alpin, A. P. Schnyder, and C. Pfleiderer, Nature (London) **594**, 374 (2021).
[33] A. Bauer, A. Neubauer, C. Franz, W. Münzer, M. Garst, and C. Pfleiderer, Phys. Rev. B **82**, 064404 (2010).
[34] A. Mishra, M. Krishnan, M. Gangrade, D. Singh, R. Venkatesh, and V. Ganesan, J. Phys.: Conf. Ser. **755**, 012037 (2016).
[35] J. Sánchez-Barriga, J. Braun, J. Minár, I. Di Marco, A. Varykhalov, O. Rader, V. Boni, V. Bellini, F. Manghi, H. Ebert, M. I. Katsnelson, A. I. Lichtenstein, O. Eriksson, W. Eberhardt, H. A. Dürr, and J. Fink, Phys. Rev. B **85**, 205109 (2012).
[36] H. Miyazaki, T. Ito, H. J. Im, S. Yagi, M. Kato, K. Soda, and S. Kimura, Phys. Rev. Lett. **102**, 227203 (2009).
[37] M. Kim and B. I. Min, Phys. Rev. B **91**, 205116 (2015).
[38] J. D. Denlinger, G.-H. Gweon, J. W. Allen, C. G. Olson, M. B. Maple, J. Sarrao, P. Armstrong, Z. Fisk, and H. Yamagami, J. Electron Spectrosc. Relat. Phenom. **117-118**, 347 (2001).
[39] J. W. Allen, J. Phys. Soc. Jpn. **74**, 34 (2005).
[40] S.-i. Fujimori, J. Phys.: Condens. Matter **28**, 153002 (2016).
[41] S. Kirchner, S. Paschen, Q. Chen, S. Wirth, D. Feng, J. D. Thompson, and Q. Si, Rev. Mod. Phys. **92**, 011002 (2020).
[42] X. Deng, K. M. Stadler, K. Haule, A. Weichselbaum, J. von Delft, and G. Kotliar, Nat. Commun. **10**, 2721 (2019).
[43] Y. Liu, H. P. Nair, J. P. Ruf, D. G. Schlom, and K. M. Shen, Phys. Rev. B **98**, 041110(R) (2018).

[44] E. Walter, K. M. Stadler, S. S. B. Lee, Y. Wang, G. Kotliar, A. Weichselbaum, and J. von Delft, Phys. Rev. X **10**, 031052 (2020).
[45] S. Doniach, Phys. B: Condens. Matter **91**, 231 (1977).
[46] S. Jang, R. Kealhofer, C. John, S. Doyle, J.-S. Hong, J. H. Shim, Q. Si, O. Erten, J. D. Denlinger, and J. G. Analytis, Sci. Adv. **5**, eaat7158 (2019).
[47] Q. Y. Chen, X. B. Luo, D. H. Xie, M. L. Li, X. Y. Ji, R. Zhou, Y. B. Huang, W. Zhang, W. Feng, Y. Zhang, L. Huang, Q. Q. Hao, Q. Liu, X. G. Zhu, Y. Liu, P. Zhang, X. C. Lai, Q. Si, and S. Y. Tan, Phys. Rev. Lett. **123**, 106402 (2019).
[48] H. Yasuoka, V. Jaccarino, R. C. Sherwood, and J. H. Wernick, J. Phys. Soc. Jpn. **44**, 842 (1978).
[49] Z. Jin, Y. Li, Z. Hu, B. Hu, Y. Liu, K. Iida, K. Kamazawa, M. B. Stone, A. I. Kolesnikov, D. L. Abernathy, X. Zhang, H. Chen, Y. Wang, C. Fang, B. Wu, I. A. Zaliznyak, J. M. Tranquada, and Y. Li, arXiv:2206.13699.
[50] Y. Nomura, S. Sakai, and R. Arita, Phys. Rev. Lett. **128**, 206401 (2022).